JACS
JOURNAL OF THE AMERICAN CHEMICAL SOCIETY
pubs.acs.org/JACS
Article

Successive Magnetic Transitions Enable an Ultrawide Temperature Window of Zero Thermal Expansion in (Hf,Ti)Fe_{2+x}

Zhao Pan,*,⊥ Haowei Zhou,⊥ Chao Chen,⊥ Yili Cao,* Xubin Ye, Ruilong Wang, Shogo Kawaguchi, Xianran Xing,* and Youwen Long*

Cite This: J. Am. Chem. Soc. 2026, 148, 12119−12125

ABSTRACT: Zero thermal expansion (ZTE) alloys hold significant potential for a variety of precise applications, yet the working temperature range remains limited, generally lower than 500 K. Herein, enabled by high-temperature annealing, we realize heterogeneous elemental distribution and thus multiple magnetic orders in nonstoichiometric kagome metal (Hf,Ti)Fe_{2+x}. Successive magnetic transitions yield ZTE in $Hf_{0.6}Ti_{0.4}Fe_{2.54}$ over an ultrawide temperature window, with an average linear coefficient of thermal expansion $\bar{\alpha}_l$ = 0.76 × 10^{-6} K^{-1} (112−525 K). Magnetization measurements, Lorentz TEM, neutron powder diffraction, and Mössbauer spectra reveal that antisite Fe introduces extra magnetic exchange interactions and stabilizes the magnetic ordering. A spin reorientation emerges near 370 K when the direction of magnetic moments in the 2*a* and 6*h* sites transform from in-plane to out-of-plane. Then, the moments show an abrupt decrease at 470 K, and turn completely paramagnetic around 525 K. The compensation between magnetic order and the phonon effect enables such an ultrawide ZTE across room temperature. The present study provides insight into unconventional ZTE behaviors for metallic magnets with promising applications.

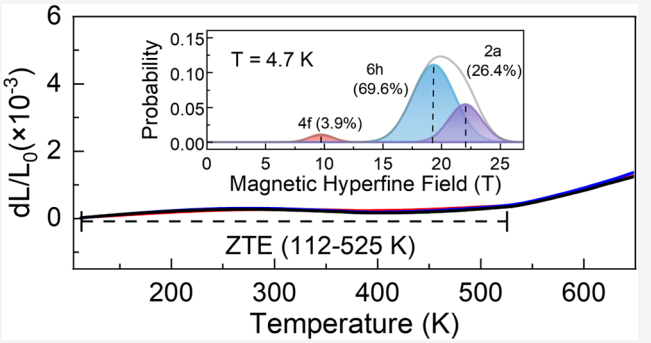

INTRODUCTION

Zero thermal expansion (ZTE) is an intriguing property of solids, characterized by their ability to maintain stable dimensions under temperature fluctuations.[1−6] ZTE alloys exhibit excellent thermal conductivity,[7] electrical conductivity,[8] and mechanical properties,[9−11] rendering them highly valuable for practical applications such as aerospace and semiconductor engineering.[12−14] Therefore, ZTE in metallic materials always arouses considerable interest. The first ZTE alloy, Invar, was discovered in 1897 and has seen widespread use over the past century.[15,16] Due to the influence of magnetic ordering on the lattice, numerous intermetallic compounds also exhibit negative thermal expansion (NTE) below the magnetic ordering temperature. Although these materials can be transformed into ZTE materials through chemical substitution, like $Mn_xFe_{5-x}Si_3$,[17] $ErFe_{10}V_{2-x}$,[18] $Fe_{2.75}Co_{0.25}PtB_{0.25}$,[19] etc.,[2,20] size effects,[21] and external-field modulation,[22] the ZTE emerges at low temperature and involves in a narrow temperature range, generally lower than 500 K. It remains a great challenge to realize a wide-temperature-window ZTE in metallic materials.

Laves-phase intermetallic compounds (AB_2) represent a large family of intermetallic compounds consisting of the kagome lattice,[23] and exhibit a wide range of physical properties, including wear-resistant and corrosion-resistant applications, hydrogen storage systems, and magnetocaloric technologies. The crystal structures of Laves phases are classified into three primary types: C14 (hexagonal, $MgZn_2$, $P6_3/mmc$), C15 (cubic, $MgCu_2$, $Fd\text{-}3m$), and C36 (hexagonal, $MgNi_2$, $P6_3/mmc$).[24,25] Their crystal structures and magnetic properties exhibit significant sensitivity to chemical composition,[26−28] making compositional tuning a key strategy for achieving ZTE performance. For example, the substitution of Fe reduces the total magnetic moment and broadens the magnetic transition temperature range in $Dy(Co_{0.89}Fe_{0.11})_2$, enabling ZTE ($\bar{\alpha}_l$ = 0.58 × 10^{-6} K^{-1}, 5−305 K).[29,30] Recently, chemical heterogeneity in Laves phases can generate ZTE over a wide temperature window, such as $Zr_{0.75}Nb_{0.25}Fe_2Co_{0.1}$ ($\bar{\alpha}_l$ = 0.79 × 10^{-6} K^{-1}, 120−440 K).[31] Despite these advances, precisely controlling the composition of different phases remains challenging.

In this study, we introduce high-temperature annealing and realize heterogeneous elemental distribution in nonstoichio-

Received: January 2, 2026
Revised: February 28, 2026
Accepted: March 4, 2026
Published: March 13, 2026

https://doi.org/10.1021/jacs.5c23372
J. Am. Chem. Soc. 2026, 148, 12119−12125

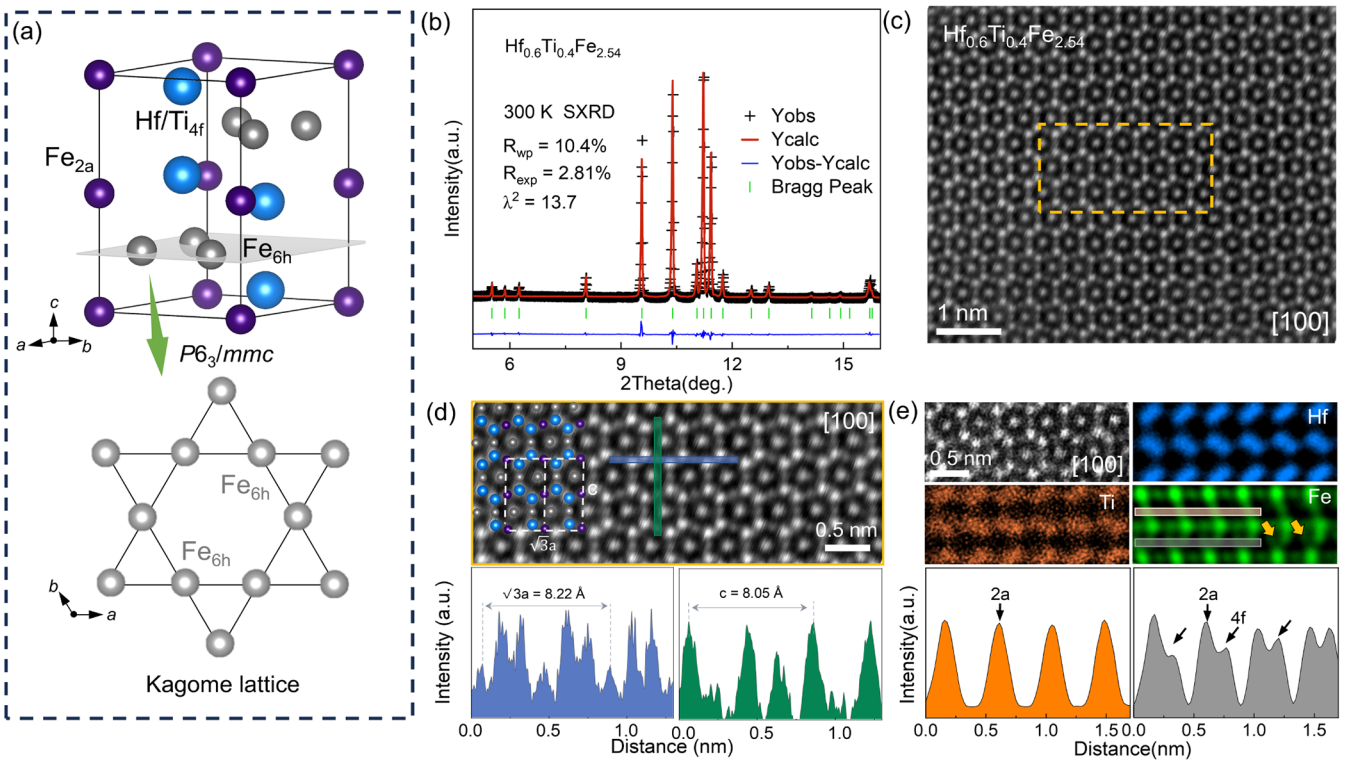

Figure 1. Crystal structure of ZTE Hf−Ti−Fe alloys. (a) The hexagonal crystal structure and Kagome lattice in (Hf, Ti)Fe_2. (b) Rietveld refinements of the SXRD patterns of $Hf_{0.6}Ti_{0.4}Fe_{2.54}$. (c) Cross-sectional HAADF-STEM image of $Hf_{0.6}Ti_{0.4}Fe_{2.54}$ along the [100] axis. (d) Enlarged STEM image in (c) and the hexagonal crystal structure model. (e) Atomically resolved energy-dispersive X-ray spectroscopy (EDXS) mappings (Hf, Ti, and Fe elements) and intensity profiles of Fe atom columns.

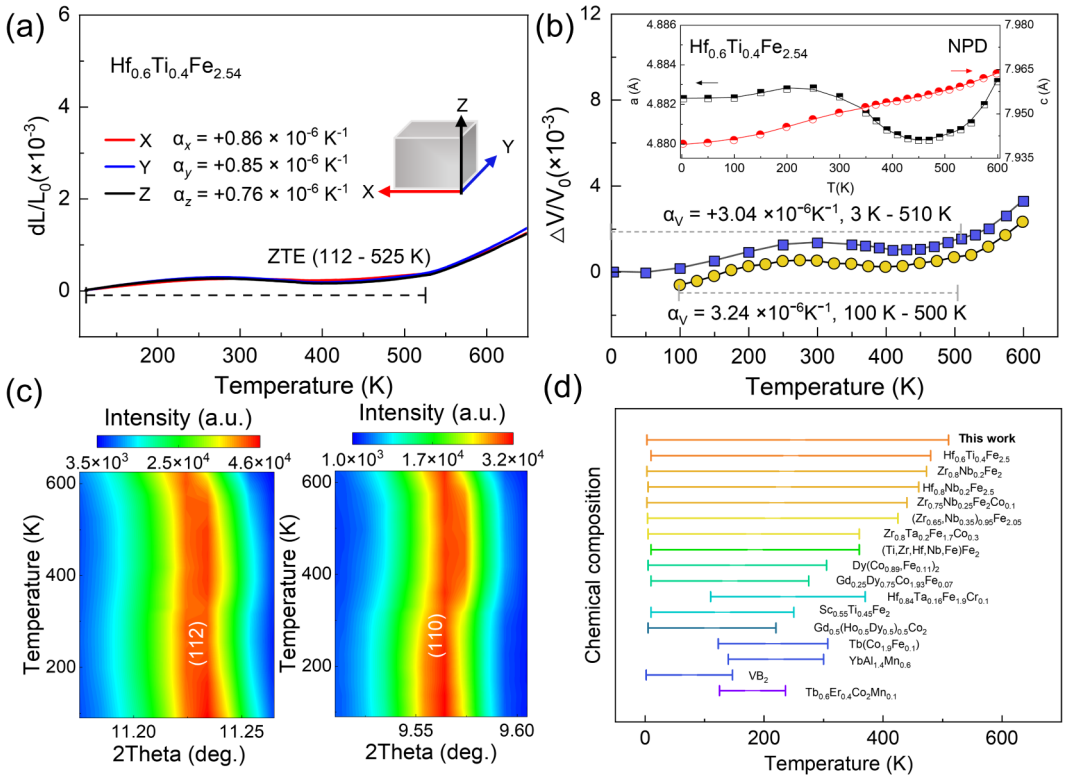

Figure 2. Thermal expansion behavior of Hf−Ti−Fe alloys. (a) Linear thermal expansion of $Hf_{0.6}Ti_{0.4}Fe_{2.54}$ along three directions. (b) Temperature dependence of NPD and SXRD-measured lattice parameters V; the inset shows the lattice parameters a and c determined by NPD. (c) Temperature dependence of the SXRD peaks (110) and (112) of $Hf_{0.6}Ti_{0.4}Fe_{2.54}$. (d) Temperature windows for conventional Laves ZTE materials.[29,31−44]

https://doi.org/10.1021/jacs.5c23372
J. Am. Chem. Soc. 2026, 148, 12119−12125

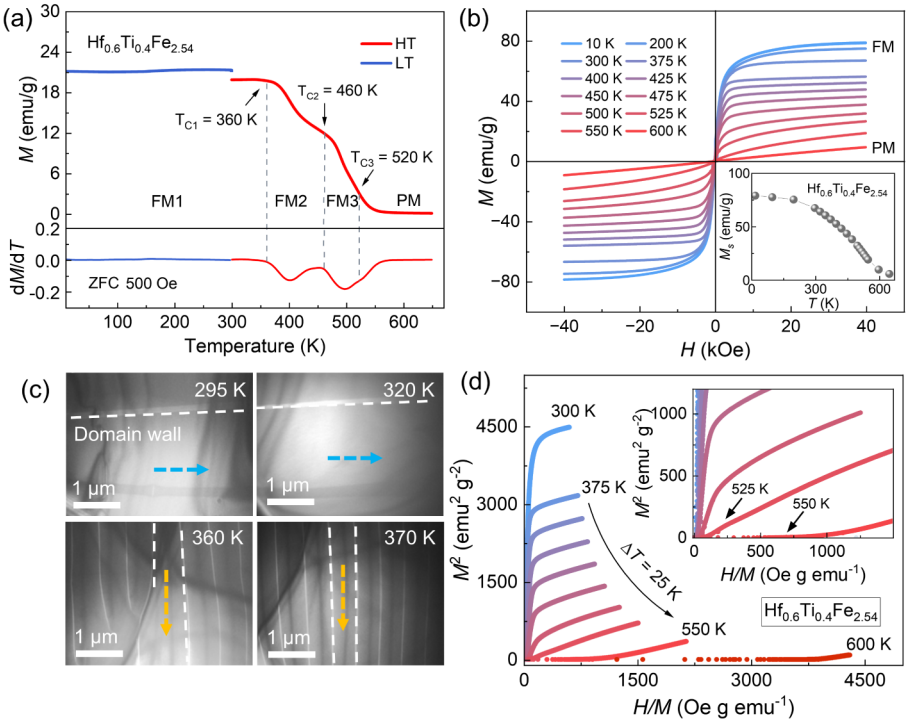

Figure 3. Magnetic behavior evolution at different temperatures of Hf−Ti−Fe alloys. (a) Temperature dependence of magnetization $M-T$ for $Hf_{0.6}Ti_{0.4}Fe_{2.54}$ in zero-field cooling under an applied magnetic field of 500 Oe. (b) Isothermal magnetization versus magnetic field curves (M-H) of $Hf_{0.6}Ti_{0.4}Fe_{2.54}$ at different temperatures, the inset shows the variation of saturation magnetization with temperature. (c) Lorentz TEM images at temperatures from 295 to 370 K. (d) Isothermal Arrott plots of $Hf_{0.6}Ti_{0.4}Fe_{2.54}$ based on the $M-H$ curves.

metric $(Hf,Ti)Fe_{2+x}$. A comprehensive study of magnetization, neutron diffraction, Lorentz TEM and Mössbauer spectroscopy revealed that antisite Fe stabilizes magnetic ordering with multiple magnetic orders. Consequently, ZTE was achieved over an ultrawide temperature range in the $Hf_{0.6}Ti_{0.4}Fe_{2.54}$ ($\overline{\alpha}_l$ = 0.76 × 10^{-6} K^{-1}, 112−525 K). The nearly isotropic ZTE in the ingot indicates its potential in future applications.

RESULTS AND DISCUSSION

As shown in Figure 1a, the $Hf_{0.6}Ti_{0.4}Fe_{2.54}$ compound exhibits a single hexagonal structure (space group: $P6_3/mmc$), with Hf and Ti atoms randomly occupying the 4*f* Wyckoff position, and Fe atoms occupying the 2*a* and 6*h* sites. The 6*h* site makes up a kagome lattice. By using 1473 K annealing for 5 days, room temperature synchrotron X-ray powder diffraction (SXRD) shows that there is negligible impurity in the as-prepared sample $Hf_{0.6}Ti_{0.4}Fe_{2.54}$, and the peak reflections index into a single Laves phase (Figures 1b, S1, and S2). The crystal structure was further confirmed via STEM along the [100] zone axis (Figure 1c). Analysis of the enlarged STEM atomic images revealed that the lattice parameters (a = 4.75 Å, c = 8.05 Å) were measured (Figure 1d), comparable to those obtained from SXRD refinement at 300 K (a = 4.8777 Å, c = 7.9463 Å). Atomic X-ray energy-dispersive spectroscopy (EDS) elemental analysis demonstrated a uniform distribution of three elements in the $Hf_{0.6}Ti_{0.4}Fe_{2.54}$ alloys (Figure 1e). Despite the introduction of excess Fe, the single-phase crystal structure was maintained. It was found that a few Fe atoms occupy the 4*f* positions (Figure 1e). The orange and gray atom peak intensity maps respectively delineate regions of uniformly distributed Fe atoms and regions where Fe atoms additionally occupy the 4*f* site.

As shown in Figure 2a, the $Hf_{0.6}Ti_{0.4}Fe_{2.54}$ exhibits favorable ZTE over a wide temperature range ($\overline{\alpha}_l$ = 0.76 × 10^{-6} K^{-1}, 112−525 K). The apparent thermal expansion of $Hf_{0.6}Ti_{0.4}Fe_{2.54}$ was measured along three directions from 112 to 525 K: $\overline{\alpha}_x$ = 0.86 × 10^{-6} K^{-1}, $\overline{\alpha}_y$ = 0.85 × 10^{-6} K^{-1}, $\overline{\alpha}_z$ = 0.76 × 10^{-6} K^{-1}, which indicates that the sample demonstrates nearly isotropic ZTE at the macroscopic bulk scale. Normal positive thermal expansion emerges upon the gradual addition of Fe (Figure S3). The evolution of SXRD peak positions with temperature further confirms the anomalous thermal expansion of the unit-cell parameters (Figures 2c and S4). The temperature dependence of the cell parameters a and c was confirmed by Rietveld refinement of the SXRD (Figures S5, S6 and Table S1) and NPD data (Figures 2b, S7 and Table S2). The cell parameter a initially increases and then decreases, while the c axis exhibits normal positive thermal expansion. The variation of unit-cell volume with temperature, obtained by calculation, is consistent with linear thermal expansion, exhibiting ZTE of $\overline{\alpha}_v$ = 3.04 × 10^{-6} K^{-1} ≈ $3\overline{\alpha}_l$. To date, most Laves ZTE materials exhibit a narrow temperature range (Figure 2d and Table S3), e.g., $Gd_{0.25}Dy_{0.75}Co_{1.93}Fe_{0.07}$[37] ($\overline{\alpha}_l$ = 0.16 × 10^{-6} K^{-1}, 10−275 K), $Sc_{0.55}Ti_{0.45}Fe_2$[38] ($\overline{\alpha}_v$ = 1.24 × 10^{-6} K^{-1}, 10−250 K), and $Zr_{0.8}Nb_{0.2}Fe_2$[44] ($\overline{\alpha}_l$ = 1.4 × 10^{-6} K^{-1}, 3−470 K). Here, in the present study, the ZTE of $Hf_{0.6}Ti_{0.4}Fe_{2.54}$ covers an ultrawide temperature range of 510 K, enhancing its potential for future applications.

To elucidate the correlation between magnetic ordering and thermal expansion, the temperature-dependent magnetization ($M-T$) of $Hf_{0.6}Ti_{0.4}Fe_{2.54}$ was measured under a 500 Oe field (Figure 3a). The $M-T$ curve reveals the existence of three distinct magnetic transition near 360, 460, and 520 K, respectively. The isothermal magnetization with magnetic field ($M-H$) curves of $Hf_{0.6}Ti_{0.4}Fe_{2.54}$ are shown in Figure 3b.

https://doi.org/10.1021/jacs.5c23372
J. Am. Chem. Soc. 2026, 148, 12119−12125

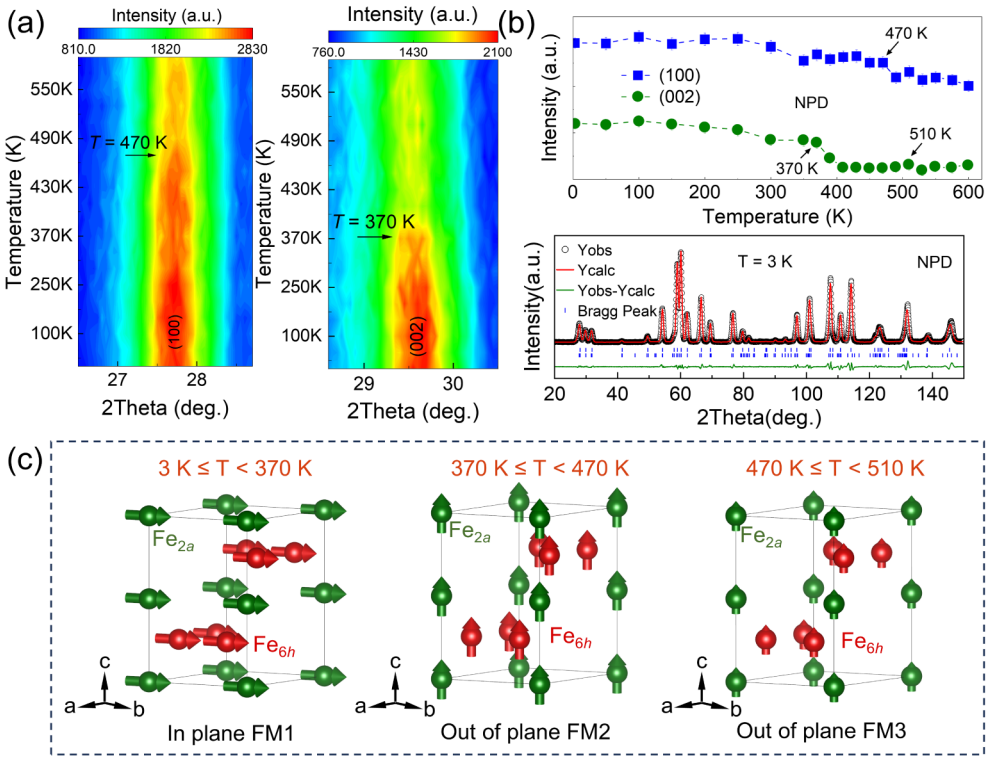

Figure 4. Magnetic structure of ZTE Hf−Ti−Fe alloys. (a) Temperature dependence of the NPD (100) and (002) peaks of $Hf_{0.6}Ti_{0.4}Fe_{2.54}$. (b) Variation of NPD peak intensities for the (100) and (002) reflections as a function of temperature, and Rietveld refinements of the NPD patterns of $Hf_{0.6}Ti_{0.4}Fe_{2.54}$ at 3 K. (c) Temperature dependence of the magnetic structure of $Hf_{0.6}Ti_{0.4}Fe_{2.54}$.

The *M*−*H* curve indicates that the sample exhibits saturation magnetization at each temperature with a very small coercive field, which demonstrates ferromagnetic (FM) ordering below 520 K. These results suggest the existence of three ferromagnetic phases, denoted as FM1, FM2, and FM3. The magnetic phase transitions are identified at critical temperatures of T_{C1} = 360 K (FM1→FM2), T_{C2} = 460 K (FM2→FM3), and T_C = 520 K (FM3→PM). To distinguish the nature of these three ferromagnetic states, Lorentz transmission electron microscopy (TEM) was performed from 295 to 370 K (Figure 3c). It indicates an obvious 90° rotation of magnetic domains around 360 K, evidencing a spin reorientation from FM1 to FM2. In the isothermal Arrott plots, the presence of curves with positive slopes indicates that the magnetic transitions are of second order, and spontaneous magnetization disappears around 525 K (Figure 3d), in agreement with the FM3-PM transition in the *M*-*T* curve. The magnetic disordering temperature coincides with the temperature at which ZTE disappears, indicating strong coupling between magnetic order and the lattice.

To further determine the magnetic structure, temperature-dependent neutron powder diffraction (NPD) was measured for $Hf_{0.6}Ti_{0.4}Fe_{2.54}$. Two significant reductions in peak intensity were observed for the (100) and (002) magnetic peaks (Figure 4a), corresponding to transitions at *T* = 370 K (from FM1 to FM2, T_{C1}) and *T* = 470 K (from FM2 to FM3, T_{C2}). The temperature dependence of the peak intensities in the NPD patterns aligns with the results of the macroscopic magnetization measurements (Figure 4b). Meanwhile, the temperature-dependent magnetic peak intensities of the (100) and (002) peaks indicate that, in addition to the transitions at 370 and 470 K, there may be another magnetic transition around 510 K, this agrees with the *M*−*T* curve (Figure 3a), namely *T* = 510 K (from FM3 to PM, T_{C3}). The detailed magnetic structures, lattice parameters, and atomic magnetic moments determined by NPD at different temperatures are shown in Figure 4c and Table S2. At low temperature, the magnetic moments of Fe_{2a} and Fe_{6h} sublattices lie within the ab-plane, remaining in-plane FM from 3 to 370 K. With the temperature increasing, all the magnetic moments of the two Fe sublattices rotate and align along the *c*-axis, thus showing out-of-plane FM2 from 370 to 470 K. Upon heating, it still demonstrates an out-of-plane ferromagnetic structure, but the magnetic moment decreases significantly from 470 to 510 K. Beyond 510 K, it transitions to the paramagnetic (PM) state. By combining macroscopic magnetic measurements, LTEM observations, and neutron diffraction results, we clearly reveal three magnetic transitions in this sample, which play a crucial role in governing its negative thermal expansion behavior.

To further investigate the spin orientation of the Fe sublattice, ^{57}Fe Mössbauer spectroscopy was performed at 4.7 and 300 K on $Hf_{0.6}Ti_{0.4}Fe_{2.54}$. At both temperatures, the spectra can be well fitted with a sextet, indicating the presence of spontaneous magnetic ordering, as shown in Figure 5a,b. At 4.7 K, the probability density function *P*(*B*) of the local magnetic field distribution shows two main peaks. The high-field peak can be further decomposed into two subpeaks with proportions of 69.6% and 26.4%, close to a 3:1 ratio, which correspond well to the relative occupancies of the two anisotropic sites (2*a* and 6*h*) in the hexagonal structure. The low-field peak originates from the antisite 4*f* positions induced by antisite Fe, accounting for about 3.9%, with a magnetic hyperfine field of 9.76 T. Upon heating to 300 K, the occupancies of the three magnetic sites (4*f*, 2*a*, and 6*h*) remain

https://doi.org/10.1021/jacs.5c23372
J. Am. Chem. Soc. 2026, 148, 12119−12125

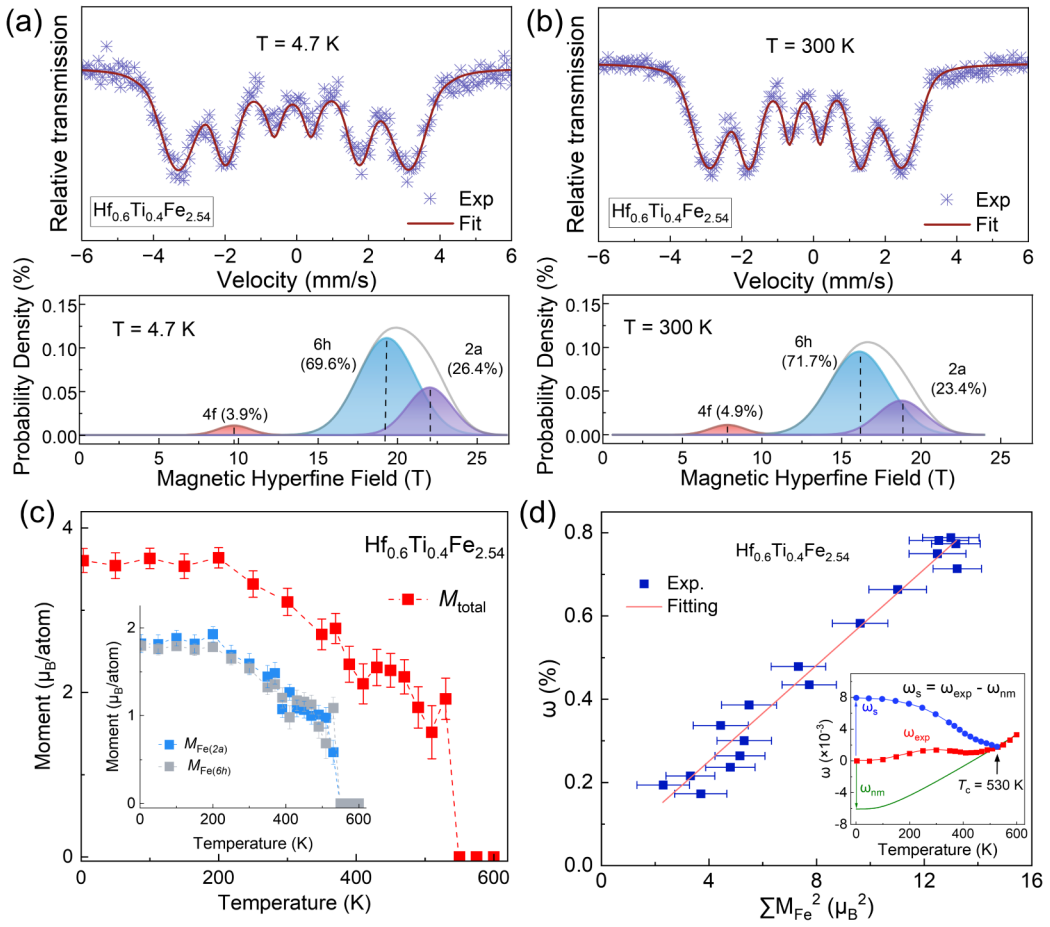

Figure 5. Mechanism of ZTE Hf−Ti−Fe alloys. The ^{57}Fe Mössbauer spectrum and hyperfine magnetic field distribution results of $Hf_{0.6}Ti_{0.4}Fe_{2.54}$ at 4.7 K (a) and 300 K (b), respectively. (c) Temperature dependence of the magnetic moments of Fe atoms at the 2*a* and 6*h* sites and of the total magnetic moment. (d) Linear relationship between the squared total magnetic moment of Fe atoms in $Hf_{0.6}Ti_{0.4}Fe_{2.54}$ and the spontaneous volumetric magnetostriction ω_s; the inset shows the procedure for calculating ω_s.

nearly unchanged, while their magnetic hyperfine fields decrease from 9.9 to 7.8 T, 19.4 to 16.2 T, and 22.1 to 18.8 T, respectively. These results indicate that the magnetic moments of the Fe sublattice gradually decrease with increasing temperature. The temperature dependences of the magnetic moments of Fe atoms at the 2*a* and 6*h* sites, and of the total magnetic moment, were determined by refinement of NPD (Figure 5c). The total magnetic moment at 3 K (3.60 μ_B/f.u.) is comparable to the saturation magnetization obtained from the $M-H$ curve at 10 K (3.77 μ_B/f.u.). The magnetic moment of Fe atoms decreases with decreases progressively with increasing temperature, reaching zero at 550 K. To investigate the contribution of magnetic order to the sample's thermal expansion, the phonon effect on lattice thermal expansion was evaluated by fitting with the Debye−Grüneisen function: $\omega_s = \omega_{exp} - \omega_{nm}$ (Figure 5d). Here, ω_{exp} denotes the experimentally determined unit-cell volume obtained from NPD data, ω_{nm} represents the nonmagnetic (phonon) contribution, which was extrapolated from the unit-cell parameters above T_C. This thereby yields the c the magnetic contribution, ω_s, to the unit-cell volume. The ZTE behavior of $Hf_{0.6}Ti_{0.4}Fe_{2.54}$ arises from the compensating contributions of phonons and magnetism to the lattice equilibrium. Furthermore, according to Landau theory, a strong correlation exists between ω_s and $M^2(T)$: $\omega_s = \kappa C M^2(T)$. Here, κ is the compressibility constant, and C is the magnetic volume coupling constant. As shown in Figure 5d, the linear relationship between ω_s and $M^2(T)$ indicates that the magnetic ordering of the Fe atoms drives the contribution of magnetism to the lattice volume.

CONCLUSIONS

In conclusion, we report a single-phase Laves-phase intermetallic compound $Hf_{0.6}Ti_{0.4}Fe_{2+x}$ that exhibits zero thermal expansion over an ultrawide temperature range ($\bar{\alpha}_l$ = 0.76 × 10^{-6} K^{-1}, 112−525 K). Comprehensive characterization of the crystal structure reveals that partial occupation of the 4*f* sites, nominally belonging to Hf/Ti, is taken up by Fe atoms. Lorentz TEM imaging, neutron powder diffraction, and Mössbauer spectroscopy indicate that antisite Fe introduces extra magnetic exchange interactions and stabilizes magnetic ordering. A spin reorientation emerges near 370 K, in which the direction of magnetic moments in the 2*a* and 6*h* sites transforms from in-plane to out-of-plane. The moment then shows an abrupt decrease at 470 K and becomes completely paramagnetic around 520 K, yielding such ultrawide ZTE. The isotropic ZTE in the ingot indicates potential for future applications.

https://doi.org/10.1021/jacs.5c23372
J. Am. Chem. Soc. 2026, 148, 12119−12125

■ ASSOCIATED CONTENT

Supporting Information

The Supporting Information is available free of charge at https://pubs.acs.org/doi/10.1021/jacs.5c23372.

Experimental and characterization methods; structural characterization including SEM and NPD/XRD; linear thermal expansion measurements; Rietveld refinement results of variable-temperature SXRD and NPD; thermal expansion coefficients of conventional Laves-phase materials, and temperature windows (PDF)

■ AUTHOR INFORMATION

Corresponding Authors

Zhao Pan − *Beijing National Laboratory for Condensed Matter Physics, Institute of Physics, Chinese Academy of Sciences, Beijing 100190, P.R. China;* orcid.org/0000-0002-8693-2508; Email: zhaopan@iphy.ac.cn

Yili Cao − *Institute of Solid State Chemistry, Department of Physical Chemistry, University of Science and Technology Beijing, Beijing 100083, P.R. China;* orcid.org/0000-0003-0523-2073; Email: yilicao@ustb.edu.cn

Xianran Xing − *Institute of Solid State Chemistry, Department of Physical Chemistry, University of Science and Technology Beijing, Beijing 100083, P.R. China;* orcid.org/0000-0003-0704-8886; Email: xing@ustb.edu.cn

Youwen Long − *Beijing National Laboratory for Condensed Matter Physics, Institute of Physics, Chinese Academy of Sciences, Beijing 100190, P.R. China;* orcid.org/0000-0002-8587-7818; Email: ywlong@iphy.ac.cn

Authors

Haowei Zhou − *Institute of Solid State Chemistry, Department of Physical Chemistry, University of Science and Technology Beijing, Beijing 100083, P.R. China*

Chao Chen − *Beijing National Laboratory for Condensed Matter Physics, Institute of Physics, Chinese Academy of Sciences, Beijing 100190, P.R. China; Key Laboratory for Intelligent Sensing System and Security of Ministry of Education, Department of Physics, Hubei University, Wuhan 430062, P.R. China*

Xubin Ye − *Beijing National Laboratory for Condensed Matter Physics, Institute of Physics, Chinese Academy of Sciences, Beijing 100190, P.R. China;* orcid.org/0000-0002-5739-8318

Ruilong Wang − *Key Laboratory for Intelligent Sensing System and Security of Ministry of Education, Department of Physics, Hubei University, Wuhan 430062, P.R. China*

Shogo Kawaguchi − *Research and Utilization Division, Japan Synchrotron Radiation Research Institute (JASRI), Sayo-cho, Hyōgo 679-5198, Japan;* orcid.org/0000-0002-8498-0936

Complete contact information is available at: https://pubs.acs.org/10.1021/jacs.5c23372

Author Contributions

⊥These authors, Z.P, H.Z., and C.C., contributed equally to this work.

Notes

The authors declare no competing financial interest.

■ ACKNOWLEDGMENTS

This research was supported by the National Key R&D Program of China (Grant No. 2021YFA1400300), the National Natural Science Foundation of China (22271309, 12425403, 22090042, 22275015, 22535001, and 12261131499), the Beijing Natural Science Foundation (Grant No. F251005), and the Fundamental Research Funds for the Central Universities, China (FRF-IDRY-23-020). The neutron diffraction experiments were performed at ECHIDNA in the Australian Nuclear Science and Technology Organization. The synchrotron radiation experiments were performed at BL02B2 in SPring-8 with the approval of the Japan Synchrotron Radiation Research Institute (JASRI) (Proposal No. 2024B1807, 2025A1495, and 2025B1628).

■ REFERENCES

(1) Van Schilfgaarde, M.; Abrikosov, I. A.; Johansson, B. Origin of the Invar Effect in Iron-Nickel Alloys. *Nature* **1999**, *400* (6739), 46−49.

(2) Rao, Z.; Tung, P.-Y.; Xie, R.; Wei, Y.; Zhang, H.; Ferrari, A.; Klaver, T.; Körmann, F.; Sukumar, P. T.; Kwiatkowski da Silva, A.; et al. Machine Learning-Enabled High-Entropy Alloy Discovery. *Science* **2022**, *378* (6615), 78−85.

(3) Sleight, A. Materials Science: Zero-Expansion Plan. *Nature* **2003**, *425* (6959), 674−676.

(4) Chen, J.; Hu, L.; Deng, J.; Xing, X. Negative Thermal Expansion in Functional Materials: Controllable Thermal Expansion by Chemical Modifications. *Chem. Soc. Rev.* **2015**, *44* (11), 3522−3567.

(5) Huang, R.; Liu, Y.; Fan, W.; Tan, J.; Xiao, F.; Qian, L.; Li, L. Giant Negative Thermal Expansion in $NaZn_{13}$-Type $La(Fe, Si, Co)_{13}$ Compounds. *J. Am. Chem. Soc.* **2013**, *135* (31), 11469−11472.

(6) Lee, C. H.; Lin, C. Y.; Chen, G. Y. Uniaxial Zero Thermal Expansion in Low-Cost Mn_2OBO_3 from 3.5 to 1250 K. *Mater. Today Phys.* **2025**, *51*, 101650.

(7) Liu, Z. K.; Wang, Y.; Shang, S. Thermal Expansion Anomaly Regulated by Entropy. *Sci. Rep.* **2014**, *4*, 7043.

(8) Dong, B.; Guo, X.; Tong, P.; Xie, L.; Liu, K.; Xiong, T.; Zhu, X.; Lin, J.; Song, W.; Sun, Y. A Zero-Thermal-Expansion Composite with Enhanced Thermal and Electrical Conductivities Resulting from 3D Interpenetrating Copper Network. *J. Alloys Compd.* **2024**, *978*, 173504.

(9) Yu, C.; Lin, K.; Zhang, Q.; Zhu, H.; An, K.; Chen, Y.; Yu, D.; Li, T.; Fu, X.; Yu, Q.; et al. An Isotropic Zero Thermal Expansion Alloy with Super-High Toughness. *Nat. Commun.* **2024**, *15* (1), 2252.

(10) Khmelevskyi, S.; Turek, I.; Mohn, P. Large Negative Magnetic Contribution to the Thermal Expansion in Iron-Platinum Alloys: Quantitative Theory of the Invar Effect. *Phys. Rev. Lett.* **2003**, *91* (3), 037201.

(11) Zhou, H.; Shen, Y.; Cao, Y.; Yang, W.; Sun, X.; Yu, C.; Lin, K.; Xing, X. A Kagome Metallic Composite Realizes Mechanically Axial Zero Thermal Expansion up to 800 K. *Adv. Mater.* **2025**, *37* (32), 2502030.

(12) Goodwin, A. L.; Calleja, M.; Conterio, M. J.; Dove, M. T.; Evans, J. S.; Keen, D. A.; Peters, L.; Tucker, M. G. Colossal Positive and Negative Thermal Expansion in the Framework Material $Ag_3[Co(CN)_6]$. *Science* **2008**, *319* (5864), 794−797.

(13) Zhang, Y.; Chen, B.; Guan, D.; Xu, M.; Ran, R.; Ni, M.; Zhou, W.; O'Hayre, R.; Shao, Z. Thermal-Expansion Offset for High-Performance Fuel Cell Cathodes. *Nature* **2021**, *591* (7849), 246−251.

(14) Song, Y.; Shi, N.; Deng, S.; Xing, X.; Chen, J. Negative Thermal Expansion in Magnetic Materials. *Prog. Mater. Sci.* **2021**, *121*, 100835.

(15) Mohn, P. A Century of Zero Expansion. *Nature* **1999**, *400* (6739), 18−19.

(16) Guillaume, C. E. Invar and Its Applications. *Nature* **1904**, *71*, 134−139.

(17) Gong, Y.; Miao, X.-F.; Samanta, T.; Taake, C.; Liu, J.; Qian, F.-J.; Shao, Y.-Y.; Zhang, Y.-J.; Ren, Q.-Y.; Caron, L.; Xu, F. Anomalous

Thermal Expansion and Enhanced Magnetocaloric Effect in < 001>-Textured $Mn_xFe_{5-x}Si_3$ Alloys. *Rare Met.* **2024**, *43* (5), 2263−2274.
(18) Li, W.; Lin, K.; Cao, Y.; Yu, C.; Wang, C. W.; Liu, X.; Kato, K.; Wang, Y.; Wang, J.; Li, Q.; Chen, J.; Deng, J.; Zhang, H.; Xing, X. Strong Coupling of Magnetism and Lattice Induces Near-Zero Thermal Expansion over Broad Temperature Windows in Er-$Fe_{10}V_{2-x}Mo_x$Compounds. *CCS Chem.* **2021**, *3* (3), 1009−1015.
(19) Cui, J.; Sun, Y.; Shi, K.; Deng, S.; Ma, T.; Du, Y.; Zhang, J.; Cheng, N.; Yuan, X.; He, L.; et al. Invar Effect in the Wide and Higher Temperature Range by Coherent Coupling in Fe-Based Alloy. *Adv. Funct. Mater.* **2023**, *34* (1), 2309431.
(20) Pan, Z.; Nishikubo, T.; Yamamoto, H.; Ye, X.; Azuma, M.; Long, Y. Negative Thermal Expansion in Metastable $PbVO_3$: High-Pressure Synthesis, Advances, and Perspectives. *cMat* **2025**, *2* (4), No. e70017.
(21) Song, X.; Sun, Z.; Huang, Q.; Rettenmayr, M.; Liu, X.; Seyring, M.; Li, G.; Rao, G.; Yin, F. Adjustable Zero Thermal Expansion in Antiperovskite Manganese Nitride. *Adv. Mater.* **2011**, *23* (40), 4690.
(22) He, J.; Pan, Z.; Su, D.; Shen, X.-D.; Zhang, J.; Lu, D.-B.; Zhao, H.-T.; Cong, J.-Z.; Liu, E.-K.; Long, Y.-W.; et al. Magnetic-Field-Induced Sign Changes of Thermal Expansion in $DyCrO_4$. *Chin. Phys. Lett.* **2023**, *40* (6), 066501.
(23) Stein, F.; Leineweber, A. Laves Phases: A Review of Their Functional and Structural Applications and an Improved Fundamental Understanding of Stability and Properties. *J. Mater. Sci.* **2021**, *56* (9), 5321−5427.
(24) Stein, F.; Palm, M.; Sauthoff, G. Structure and Stability of Laves Phases. Part I. Critical Assessment of Factors Controlling Laves Phase Stability. *Intermetallics* **2004**, *12* (7−9), 713−720.
(25) Asano, S.; Ishida, S. Magnetism and Crystal Structure of Laves Phase Compounds. *J. Phys. F* **1988**, *18* (3), 501−515.
(26) Rechenberg, H. R.; Morellon, L.; Algarabel, P. A.; Ibarra, M. R. Magnetic Moment at Highly Frustrated Sites of Antiferromagnetic Laves Phase Structures. *Phys. Rev. B* **2005**, *71* (10), 104412.
(27) Yibole, H.; Pathak, A. K.; Mudryk, Y.; Guillou, F.; Zarkevich, N.; Gupta, S.; Balema, V.; Pecharsky, V. K. Manipulating the Stability of Crystallographic and Magnetic Sub-Lattices: A First-Order Magnetoelastic Transformation in Transition Metal Based Laves Phase. *Acta Mater.* **2018**, *154*, 365−374.
(28) Xu, J.; Wang, Z.; Huang, H.; Li, Z.; Chi, X.; Wang, D.; Zhang, J.; Zheng, X.; Shen, J.; Zhou, W.; et al. Significant Zero Thermal Expansion Via Enhanced Magnetoelastic Coupling in Kagome Magnets. *Adv. Mater.* **2023**, *35* (8), 2208635.
(29) Wang, J.-N.; Hu, F.-X.; Wang, B.-J.; Tian, Z.-Y.; Sun, C.-Z.; Wang, J.-T.; Huang, Q.-Z.; Wang, J.; Chen, Y.; Sun, J.; et al. Phase Transition Modulation and Wide Temperature Interval Zero Thermal Expansion in $Dy(Co_{1-x}Fe_x)_2$ Compounds. *Rare Met.* **2025**, *44* (11), 8911−8923.
(30) Li, B.; Luo, X. H.; Wang, H.; Ren, W. J.; Yano, S.; Wang, C. W.; Gardner, J. S.; Liss, K. D.; Miao, P.; Lee, S. H.; Kamiyama, T.; Wu, R. Q.; Kawakita, Y.; Zhang, Z. D. Colossal Negative Thermal Expansion Induced by Magnetic Phase Competition on Frustrated Lattices in Laves Phase Compound $(Hf,Ta)Fe_2$. *Phys. Rev. B* **2016**, *93* (22), 224405.
(31) Sun, Y.; Yu, R.; Khmelevskyi, S.; Kato, K.; Cao, Y.; Hu, S.; Avdeev, M.; Wang, C.-W.; Yu, C.; Li, Q.; et al. Local Chemical Heterogeneity Enabled Superior Zero Thermal Expansion in Nonstoichiometric Pyrochlore Magnets. *Natl. Sci. Rev.* **2025**, *12* (3), nwae462.
(32) Sun, Y.; Cao, Y.; Ren, Y.; Lapidus, S. H.; Li, Q.; Deng, J.; Miao, J.; Lin, K.; Xing, X. Structure, Magnetism and Low Thermal Expansion in $Tb_{1-x}Er_xCo_2Mn_y$ Intermetallic Compounds. *Microstructures* **2023**, *3*, 2023028.
(33) Cao, Y.; Ji, W.; Lin, K.; Lin, H.; Li, Q.; Wang, C. W.; Wang, N.; Deng, J.; Chen, J.; Xing, X. Zero Thermal Expansion and Strong Covalent Binding of VB_2 Compound. *Inorg. Chem.* **2021**, *60* (14), 10095−10099.
(34) Wang, H.; Xu, Y.; Song, Y.; Sanson, A.; Zhang, Y.; Yao, Y.; Liu, H.; Watanabe, T.; Zeng, J.; Shi, N.; Chen, J. Isotropic Zero Thermal Expansion in $Yb(Al,Mn)_2$: Achieving Continuous Shiftability over a Wide Temperature Range. *J. Am. Chem. Soc.* **2025**, *147* (38), 34697−34705.
(35) Song, Y.; Chen, J.; Liu, X.; Wang, C.; Zhang, J.; Liu, H.; Zhu, H.; Hu, L.; Lin, K.; Zhang, S.; Xing, X. Zero Thermal Expansion in Magnetic and Metallic $Tb(Co,Fe)_2$ Intermetallic Compounds. *J. Am. Chem. Soc.* **2018**, *140* (2), 602−605.
(36) Hao, J. Z.; Shen, F. R.; Hu, F. X.; Zhou, H. B.; Yu, Z. B.; Gao, Y. H.; Liang, W. H.; Qiao, K. M.; Wang, B. J.; Li, J.; Zhang, C.; Wang, J.; He, L. H.; Liang, T. J.; He, J.; Sun, J. R.; Shen, B. G. Realization of Ultra-Low Thermal Expansion over a Broad Temperature Interval in $Gd_x(Dy_{0.5}Ho_{0.5})_{1-x}Co_2$ Compounds. *Scr. Mater.* **2020**, *185*, 181−186.
(37) Song, Y.; Sun, Q.; Xu, M.; Zhang, J.; Hao, Y.; Qiao, Y.; Zhang, S.; Huang, Q.; Xing, X.; Chen, J. Negative Thermal Expansion in $(Sc,Ti)Fe_2$ Induced by an Unconventional Magnetovolume Effect. *Mater. Horiz.* **2020**, *7* (1), 275−281.
(38) Hu, J.; Lin, K.; Cao, Y.; Yu, C.; Li, W.; Huang, R.; Fischer, H. E.; Kato, K.; Song, Y.; Chen, J.; Zhang, H.; Xing, X. Adjustable Magnetic Phase Transition Inducing Unusual Zero Thermal Expansion in Cubic RCo_2-Based Intermetallic Compounds (R = rare earth). *Inorg. Chem.* **2019**, *58* (9), 5401−5405.
(39) Li, J.; Lin, K.; Xu, H.; Yang, W.; Zhang, Q.; Yu, C.; Zhang, Q.; Chen, J.; Wang, C. W.; Kato, K.; Kawaguchi, S.; You, L.; Cao, Y.; Li, Q.; Chen, X.; Miao, J.; Deng, J.; Xing, X. High-Entropy Magnet Enabling Distinctive Thermal Expansions in Intermetallic Compounds. *J. Am. Chem. Soc.* **2024**, *146* (44), 30380−30387.
(40) Li, W.; Lin, K.; Yan, Y.; Yu, C.; Cao, Y.; Chen, X.; Wang, C.-W.; Kato, K.; Chen, Y.; An, K.; et al. A Seawater-Corrosion-Resistant and Isotropic Zero Thermal Expansion $(Zr,Ta)(Fe,Co)_2$ Alloy. *Adv. Mater.* **2022**, *34* (34), 2109592.
(41) Sun, Y.; Cao, Y.; Hu, S.; Avdeev, M.; Wang, C. W.; Khmelevskyi, S.; Ren, Y.; Lapidus, S. H.; Chen, X.; Li, Q.; Deng, J.; Miao, J.; Lin, K.; Kuang, X.; Xing, X. Interplanar Ferromagnetism Enhanced Ultrawide Zero Thermal Expansion in Kagome Cubic Intermetallic $(Zr,Nb)Fe_2$. *J. Am. Chem. Soc.* **2023**, *145* (31), 17096−17102.
(42) Dong, X.; Lin, K.; Yu, C.; Zhang, W.; Li, W.; Zhang, Q.; Zhang, Q.; Liu, J.; Cao, Y.; Xing, X. Zero Thermal Expansion in Non-Stoichiometric and Single-Phase $(Hf,Nb)Fe_{2.5}$ Alloy. *Scr. Mater.* **2023**, *229*, 115388.
(43) Song, Y.; Sun, Q.; Yokoyama, T.; Zhu, H.; Li, Q.; Huang, R.; Ren, Y.; Huang, Q.; Xing, X.; Chen, J. Transforming Thermal Expansion from Positive to Negative: The Case of Cubic Magnetic Compounds of $(Zr,Nb)Fe_2$. *J. Phys. Chem. Lett.* **2020**, *11* (5), 1954−1961.
(44) Lin, K.; Zhang, W.; Yu, C.; Sun, Q.; Cao, Y.; Li, W.; Jiang, S.; Li, Q.; Zhang, Q.; An, K.; Chen, Y.; Yu, D.; Liu, J.; Kato, K.; Zhang, Q.; Gu, L.; Kuang, X.; Tang, Y.; Miao, J.; Xing, X. Chemical Heterogeneity Modulated Zero Thermal Expansion Alloy over Super-Wide Temperature Range. *Cell Rep. Phys. Sci.* **2023**, *4* (2), 101254.

https://doi.org/10.1021/jacs.5c23372
J. Am. Chem. Soc. 2026, 148, 12119−12125